

TS-DRN: An EEG Recognition Algorithm for Art Design Decisions Making

Lijuan Shen, Jingmin Yang, Meiyuan Xu, and Bokai Yang

Abstract—Electroencephalogram (EEG) technology is vital in art design decisions making and has become a prevalent research trend. However, With the temporal variability in EEG signals, there is a problem of low model prediction accuracy. Therefore, We propose an EEG signal recognition algorithm called the Time-Slicing and Deep Residual Network (TS-DRN). First, we present the subjects with the patterns of different styles of designs to capture their EEG signals. Second, we employ the time-slicing strategy to process the original signal, enhancing the number of training samples and reducing the sample features' dimensionality. Finally, we use the combined EEG feature maps as inputs to the deep residual network to obtain the classification results. Our experimental results demonstrate that this paper's EEG signal classification accuracy is 85.8%, demonstrating our method's effectiveness for EEG signal classification.

Index Terms—Design Decisions, EEG, Residual Network, Time-slicing

I. INTRODUCTION

DESIGN decisions are crucial in determining whether a product can successfully enter the market [1]. However, this process is subjective and uncertain since design decisions are often affected by factors such as the decision-makers' academic backgrounds and personal preferences [2]. Many studies have tried various methods to solve this problem. For example, Antioco et al. [3] combined data from interviews, questionnaires, and feedback sessions to narrow the gap between decisions and actual ideas. Zhang et al. [4] utilized sales data for forecasting customer product choices. Ireland and Liu [5] proposed a design framework to help designers make relatively objective decisions by analyzing online product reviews. Peng et al. [6] built a green building design decision-making system based on ontology and case reasoning technology, which significantly improved the design quality of green buildings by integrating experts' experiences and case knowledge. Although the above-related researches have achieved specific results, they have yet to reveal the neural mechanisms behind design decisions.

Manuscript received July 10, 2023; revised December 16, 2023. This work was supported in part by the Fujian Province Nature Science Foundation under Grant No. 2020J01813, the Research Project on Education and Teaching Reform of Undergraduate Colleges and Universities in Fujian Province under Grant FBJG20210070, and the 2022 Annual Project of the Fourteenth Five-Year Plan for Fujian Educational Science (No. FJJKBK22-173).

Lijuan Shen is a graduate student of School of Computer Science and Engineering, Minnan Normal University, Zhangzhou 363000, China (e-mail: 17806288215@163.com).

Jingmin Yang is a professor of School of Computer Science and Engineering, Minnan Normal University, Zhangzhou 363000, China (corresponding author to provide phone: 188-5965-7273; e-mail: yjm1758@mnnu.edu.cn).

Meiyuan Xu is an associate professor of School of Computer Science and Engineering, Minnan Normal University, Zhangzhou 363000, China (e-mail: plum-xu@163.com).

Bokai Yang is an associate professor of School of Arts, Minnan Normal University, Zhangzhou 363000, China (e-mail:79290771@qq.com).

The electroencephalogram (EEG) [7] results from the synchronous occurrence of postsynaptic potentials in numerous neurons during brain activity. The study [8] has shown that users' preferences for product design schemes can be reflected in EEG signals. The EEG can collect different EEG signals when the subject makes different decisions. Therefore, many studies used EEG to record EEG signals while subjects were making design decisions[9]. By analyzing the EEG signals of decision makers during the design decision-making process, researchers can better understand the psychological state behind the decision makers [10]. Additionally, the relative objectivity of EEG signals can neutralize the subjectivity of the decision-making [11]. Thus, various investigations [12] have sought to quantify design decisions alongside EEG monitoring during subjects' decision-making.

In our research, we formulate an art design decision-making framework and enlist participants based on a prior relevant investigation [13]. Before starting the experiment, we explain the experimental process and requirements to the subjects. Then, we wear subjects with the EEG signal acquisition equipment. Throughout the experiment, the system records each subject's decision-making results and the EEG signal data. Later, we preprocess the raw EEG signal to obtain the cleaner signal as the input to the Time-Slicing and Deep Residual Network (TS-DRN) model. After extensive training sessions, our model attains an average accuracy in classification of 85.8%. The performance of our proposed model surpasses that of comparable studies. The primary contributions of this paper include the following:

(1) This paper introduces a design decision-making approach grounded in EEG signals. The method quantifies subjective decision-making and enhances the reliability and researchability. It makes the decision-making results more scientific and objective.

(2) This paper proposes the TS-DRN model to address the issues of high feature dimensionality and complex feature extraction in EEG signals. This model increases the quantity of training instances while decreasing each sample's feature dimensionality. Additionally, it autonomously extracts data features, eliminating the necessity for manual feature extraction. The findings indicate an enhancement in our model's classification accuracy of EEG signals, resulting in an average accuracy of 85.8%.

The structure of this paper is outlined as follows: Section II provides an overview of the existing status of EEG research. Section III outlines the EEG data collection procedure and the network structure. Section IV delves into the analysis of the experimental results. Section V reviews and discusses related studies. Section VI provides a comprehensive summary of the paper and explores future directions.

II. RELATED WORK

In recent years, several research results have been achieved by applying EEG signals to design decisions. Chew et al. [14] employed EEG to gauge users' aesthetic inclinations towards 3D shapes. Lou et al. [15] introduced the Kano model, which leveraged real-time EEG signals to analyze subjects' mental states. This approach empowers designers to understand subjects' needs more accurately and nuancedly. Lou et al. [16] gathered and examined EEG signals from subjects during elevator rides to assess different elevator design schemes. Golnar-Nik et al. [17] captured EEG signals during subjects' exposure to advertisements for different cell phone brands, aiming to forecast consumer decision-making behavior. Kumar et al. [18] proposed a rating prediction framework that combines product reviews and EEG data to predict subjects' ratings for unknown products. Chang et al. [19] proposed an extended short-term memory network model to recognize users' decision-making EEG signals. Jiao et al. [20] concluded that EEG signals could serve as evaluation indicators for design decisions by analyzing decision-makers' EEG signals related to car front-end styling preferences.

In recent years, various methods of categorizing EEG signals have emerged. Bhardwaj et al. [21] employed support vector machines (SVMs) and linear discriminant analysis (LDA) algorithms for the classification of EEG signals. Zhou et al. [22] employed a multilinear regression approach to classify EEG signals related to motor intention. Krishnandhika et al. [23] employed an enhanced neural network based on radial basis functions as the classifier to identify patterns in EEG data. Geng et al. [24] utilized wavelet transform for the extraction of EEG characteristics, which were subsequently fed into diverse classification models within computational intelligence to discern varying degrees of dizziness. Chen et al. [25] combined EEG, electromyography (EMG), and electrocardiography (ECG) signals to evaluate the severity of stroke patients. Although machine learning has progressed in classifying EEG signals, researchers must possess extensive practical experience and prior knowledge, as manual extraction of EEG characteristics is required. Deep learning has emerged as a powerful tool capable of autonomously identifying intricate data features, and an increasing number of investigations have initiated the integration of deep learning methodologies into the classification of EEG signals. Chen et al. [26] employed graph neural networks (GNN) for the categorization of EEG signals recorded during simulated driving scenarios. Zhang et al. [27] introduced a convolutional neural network (CNN) designed to process multiple perspectives in the context of EEG signal classification. Tripathi et al. [28] utilized deep convolutional neural networks (DCNN) in their investigations of binary emotion classification using the DEAP dataset. Song et al. [29] transformed collected EEG signals during motor imagery into two-dimensional video-like images, and they input them into a convolutional neural network-extreme learning machine model for classification. Although previous researches have achieved a series of results, the small size of the EEG dataset can easily lead to overfitting, thereby reducing the classification accuracy. This paper incorporates residual blocks [30] into the CNN architecture to overcome

this challenge. This integration helps alleviate overfitting issues and enhances the model's capacity to grasp the unique features inherent in EEG data effectively, consequently boosting the accuracy of EEG signal classification.

Despite the advancements brought about by deep learning in enhancing the accuracy of EEG signal classification, challenges persist, including constraints related to limited sample sizes and high-dimensional features [31]. These challenges are exacerbated by the pronounced temporal variability [32] inherent in EEG signals. Therefore, many studies [33-43] have used a sliding window to crop the EEG data. They sliced samples into smaller pieces to increase the sample quantity and reduce the dimensionality of data features. The window sizes employed in various studies were not fixed, which ranged from 1 second to 60 seconds. However, Candra et al. [43] discovered that the size of the EEG signal segments is not necessarily better when smaller. They explored the effect of different window sizes on the classification of EEG signals. They found that the accuracy in classifying EEG data when employing a window size ranging from 3 to 12 seconds surpassed that of the original samples before segmentation. Besides, merely cutting the EEG data into smaller segments does not guarantee that the neural network can effectively learn and extract the correlation features among individual slices. Thus, we propose the Time-Slicing strategy for slicing EEG data samples. Instead of using a variable window size, we set the window size as a constant between 3-12 seconds. And then, we adjust the move step size to be smaller than the window size to ensure that the CNN can extract the associated features of overlapping parts and find the optimal time-slicing.

Although CNN has been widely applied in classifying EEG signals, most studies still employ laborious preprocessing techniques and manual feature extraction for EEG signals. These methods do not reflect the advantage of CNN in automatically learning EEG signal features. Therefore, we present an integrated model, the Time-Slicing and Deep Residual Networks (TS-DRN), tailored explicitly for art design decision-making. This model considers the advantage of deep residual networks for automatically extracting EEG features. Additionally, it uses the Time-Slicing segmentation to reduce the temporal feature dimensionality, resulting in improved classification accuracy for EEG signals. Our model extracts EEG features. It reduces the dependence of the model on manually extracted features. Furthermore, it improves the classification accuracy of EEG signals. Overall, our model has broad application prospects in EEG signal classification and plays a vital role in the art design decision field.

III. METHOD

A. Data collection

1) *Collecting equipment:* We use brain electrodes to capture EEG signals. This device is from Beijing Jinfa Technology Company. It has 32 electrodes. Its sampling frequency is 256Hz. The collected EEG data are presented in real-time on the ErgoLAB's cloud system for synchronizing human-machine environments.

2) *Subjects:* There are 16 subjects in this experiment, including 9 men and 7 women. Their median age is 22. All

of them have bachelor's degrees or above. Each subject takes approximately 10 minutes to complete the experiment.

3) *Experimental materials*: The Eight Treasures Printing Clay is one of the three treasures in Zhangzhou, an ancient city with a rich history and culture. Also, it is one of the intangible heritage of China. The experimental materials of this paper are the packaging design schemes of four kinds of Eight Treasures printing clay, as shown in Fig. 1. The first design scheme, named "Zhangzhou Daffodil". The entire scheme's primary color palette consists of red and yellow, complemented by elements of traditional Minnan architecture, daffodil flowers, and Minnan floral tiles. Its made of degradable material, aligning with the principles of sustainable development. The second design option is called "Ethnic Minorities". It uses elements of the She ethnic minority, which is the most distributed in southern Fujian, as the main element of the design. The handbag is designed with ethnic images, and the box uses the surname Lan, one of the four surnames of the She ethnic group, to form a connection with the handbag. The entire plan fully demonstrates the characteristics of the She culture and also reflects the inclusiveness of multiculturalism. The third design plan is called "Minnan Tulou". It uses the white and dark red as the main colors, echoing the color of the ink pad. The wooden window pattern of ancient folk houses in southern Fujian is the background pattern of the design scheme. The southern Fujian earth building is its main motifs. The box body uses a lacquered wood flip cover and a horn hook lock, which represents the essence and inheritance of traditional Chinese culture. The entire design scheme shows the unique cultural charm of southern Fujian, and also reflects the respect and inheritance of traditional culture. The fourth design scheme is called "Chinese Pagoda". The main elements of its outer packaging are dragon towers and daffodils. Longwen Pagoda is a landmark building in Zhangzhou. Narcissus is the city flower of Zhangzhou and the provincial flower of Fujian, which means that the eight-treasure ink pad can be as fragrant as the fragrance of narcissus. The inner packaging box mainly uses golden yellow as the background color, supplemented by dragon and phoenix patterns. The golden color was only used by the royal family in ancient China, representing the majesty of the royal family, while the dragon and phoenix patterns represented that the Eight Treasures Ink Clay was once used by the royal family. Now, the dragon and phoenix also symbolize the rebirth of the phoenix, representing the indomitable and strong will of the Chinese nation. The entire design scheme fully demonstrates the noble quality and historical and cultural value of Babao ink pad.

4) *Data collection process*: Before the experiment, we ask the subjects to fill out a personal information form and inform them about the experimental details. Then, we place electrodes on the subjects' heads to record their EEG signals while they decide on four schemes. After completing the above experimental preparations, we start the experiment. First, the subjects rest for 60 seconds. Then, the four design schemes are played on the screen randomly, each lasting 14 seconds with a 3-second interval between each pair of schemes. Next, the specific rules for making decisions are displayed on the screen, instructing the subjects to assign any integer from 0 to 9 (with 9 indicating their favorite)



Fig. 1. Packaging schemes of Eight Treasures printing clay

to each scheme. Finally, the subjects make decisions and rate them. Based on the scores from high to low, we label the corresponding EEG signals as 0 to 3. The dataset we collected is named the "Art dataset". The entire data collection process is illustrated in Fig. 2.

B. TS-DRN model

The overall representation of the TS-DRN model can be observed in Fig. 3. It consists of three main components: the EEG data capture, Time-slicing, and deep residual networks. First, we remove industrial frequency signals from the collected EEG data. Then, we adopt the time-slicing strategy to segment the collected EEG data. This strategy maintains a constant size for the sliding window, varying the step size while keeping its length less than or equal to the window size. Time slices at different step lengths generate various EEG signal features. Finally, we input these different features into our proposed deep residual network to classify them. In the process of capturing EEG signals, 50 Hz power frequency noise is introduced due to the interference of power lines, affecting the quality of the EEG signals. Therefore, we pre-process the data using a Butterworth filter, which eliminates the 50 Hz industrial frequency and enhances the signal-to-noise ratio. Its formula is:

$$H(u, v) = \frac{1}{1 + \left[\frac{D(u, v)w}{D^2(u, v) - D_0^2} \right]^{2n}} \quad (1)$$

where D_0 represents the distance between the frequency point to be blocked and the frequency center, w is the bandwidth of the Butterworth filter, and n represents the order of the Butterworth filter.

1) *Time-slicing strategy*: This work introduces a sample slicing approach termed the Time-Slicing strategy, illustrated in Fig. 4. The Time-Slicing strategy sets the time window as a constant w and the step as a variable s . We make $s \leq w$ and divide the data samples into different time sequence slices. Then, we input these slices to our classifier for classification,

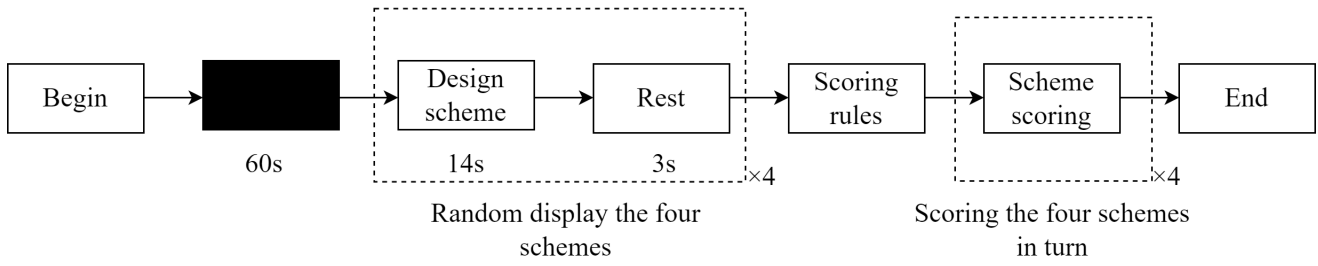


Fig. 2. EEG data collection process

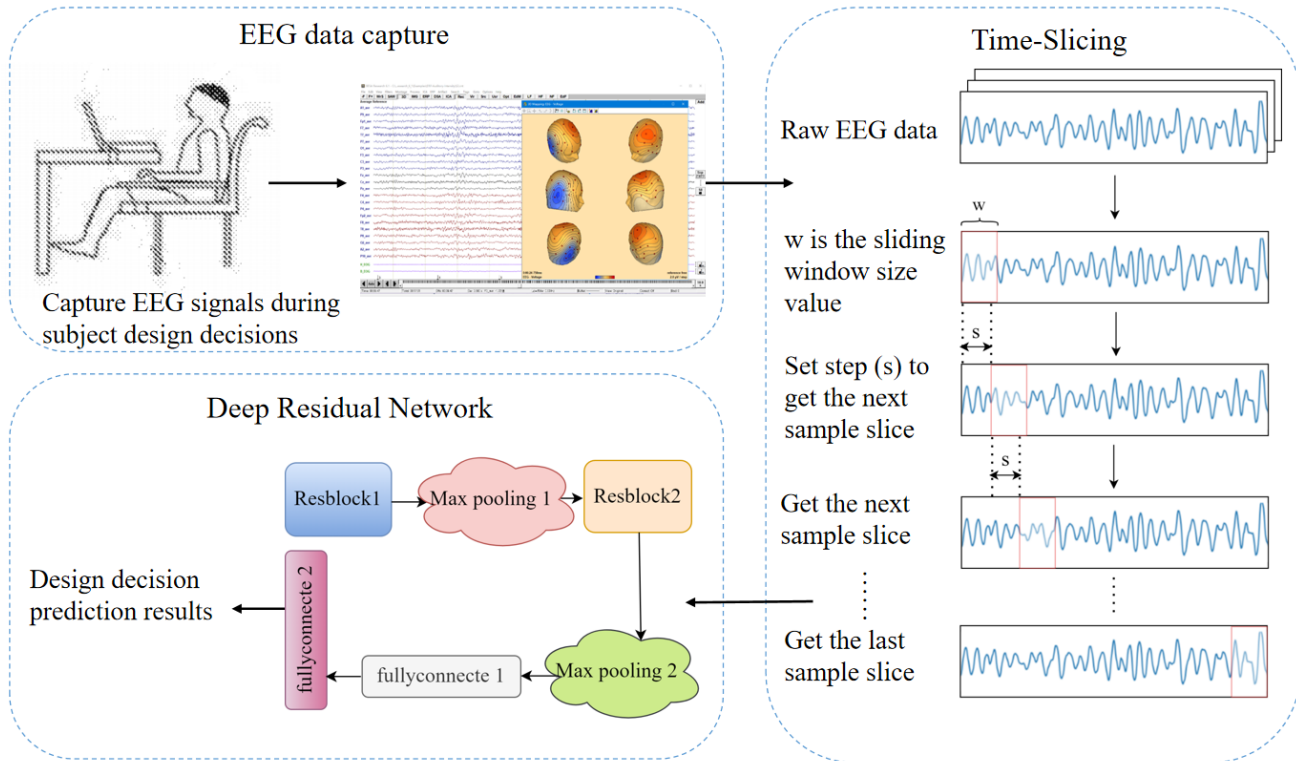


Fig. 3. TS-DRN model

and we can obtain the optimal time sequence slice with the highest classification accuracy. Afterward, we select the optimal time sequence slices as the EEG features and use them in the subsequent experiments. The strategy uses slices to solve the problem of the small amount of EEG sample data. In addition, the step size in the strategy is configured to be less than the size of the sliding window, ensuring that adjacent slices exhibit overlapping features. Therefore, our strategy also resolves the issue of regular sample slicing methods that overlook the continuity among samples. The Time-Slicing strategy can divide the original EEG data into smaller segments for each experimental data sample X^i based on the given parameter values w and s . The formula for the Time-Slicing method is as follows:

$$O_t^i = \{X_{1, \dots, t, \dots, t+w}^i | t = 1, 1 + w, \dots, 1 + nw\} \quad (2)$$

where $n = 1 + (T - s)/w$, indicates that the original input time domain data sequence is cut into n copies.

2) *Deep residual network*: The classifier in this paper is a deep residual network based on CNN, as shown in Fig. 5. The network encompasses six convolutional layers, two max pooling layers, a flattened layer, and integrates

two fully connected layers. We construct three convolutional blocks as one residual block where the sum of the first two convolutional blocks is the input to the third convolutional block. There are two residual blocks in our network. We use the properties of Maxout to enhance our model's expressive power and fitting ability. Furthermore, we use a central loss function to strengthen the robustness of the model. Finally, we use the softmax function as the output function and optimize it using the Adam optimizer. The convolution layer can extract local features from the input data through convolution operation. It simplifies the process of EEG feature extraction. Then, The convolution kernel and the input feature maps make a convolution operation. Afterwards, we use activation functions to obtain nonlinear feature factors and increase the expressive power of the model. The convolution kernel size of the convolutional layer in this paper is 3×3 , and the stride is 1. The formula for calculating the feature map is as follows:

$$OUT_{length} = \frac{in_{length} - k_{length} + 2P}{stride_{length}} + 1 \quad (3)$$

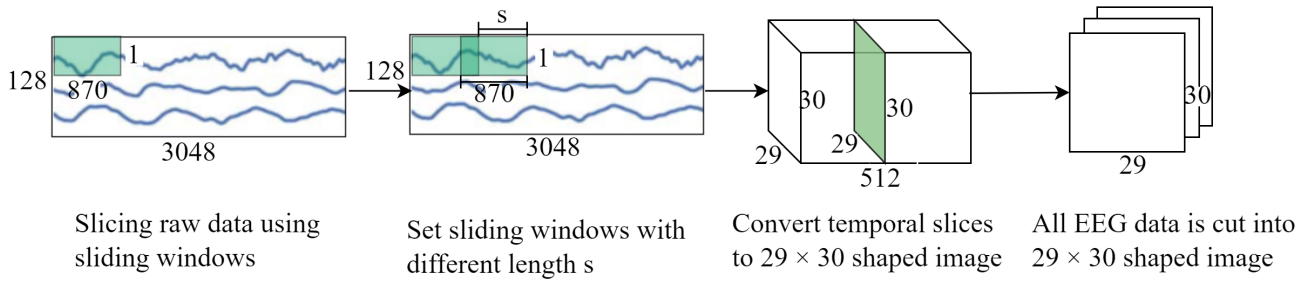


Fig. 4. Time-slicing strategy

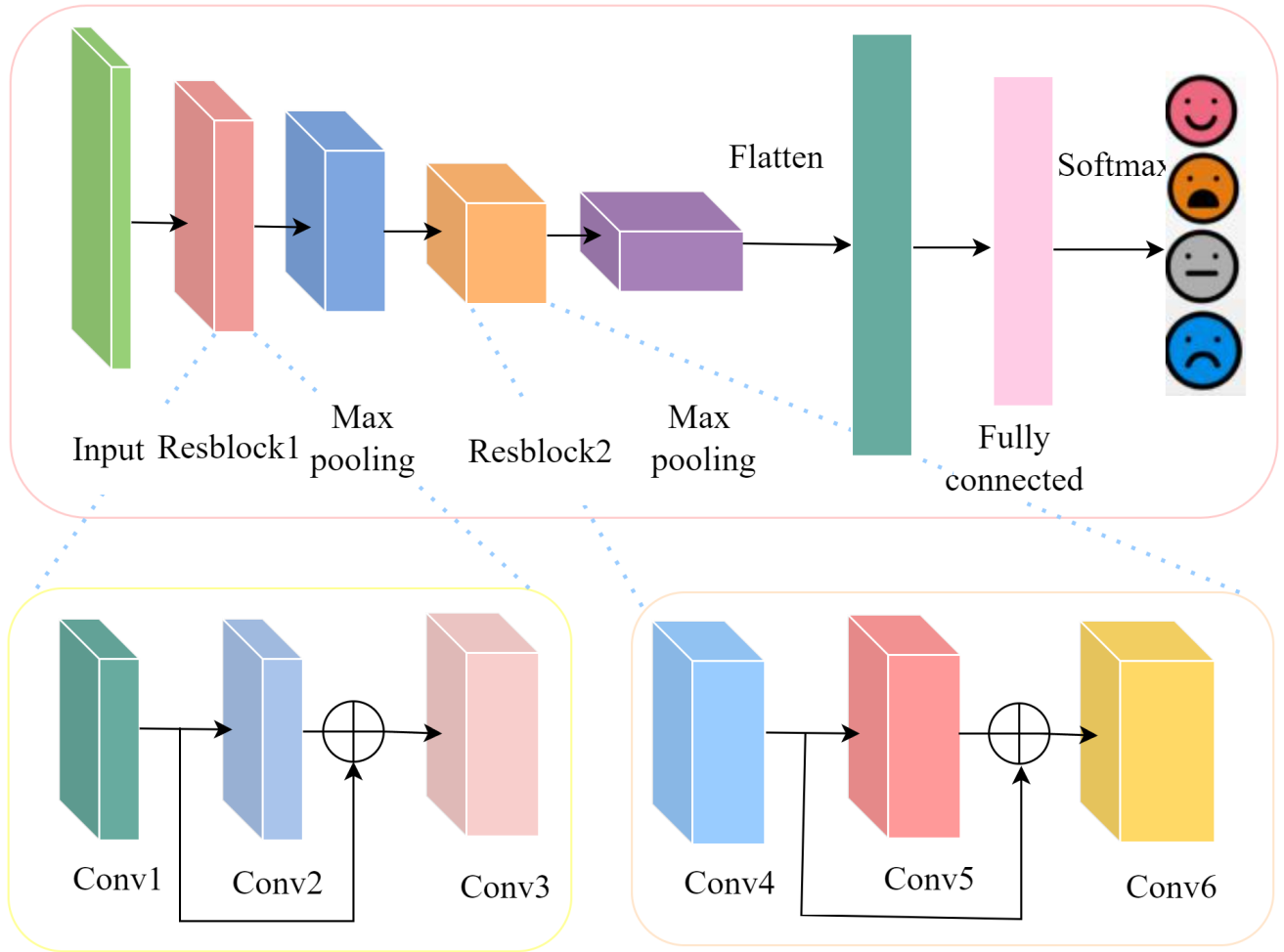


Fig. 5. Deep residual network

$$OUT_{width} = \frac{in_{width} - k_{width} + 2P}{stride_{width}} + 1 \quad (4)$$

where OUT_{length} and OUT_{width} are the length and width of the feature map after convolution of input data, in_{length} and in_{width} are the longness and wideness of the feature map input to the convolutional layer, k_{length} and k_{width} are the length and width of the convolutional kernel, P is the number of edge padding zeros, $stride_{length}$ and $stride_{width}$ are the horizontal and vertical movement steps of the convolution kernel.

We employ the maxout function as the activation mechanism in the model. It is a relatively common activation function with high flexibility and generalization ability. In

contrast to conventional activation functions such as the sigmoid functions, the maxout function has superior adaptability to process diverse data types and intricate model architectures. The formula for the maxout function is as follows:

$$Z_{ij} = X_a^T W_{\dots ij} + b_{ij}, W \in R^{d \times m \times k} \quad (5)$$

$$M_{i(x)} = \max Z_{ij}, j \in [1, k] \quad (6)$$

where X_a is the input data, while the weight coefficients W has dimensions of (d, m, k) , d refers to the number of input features, m represents the quantity of features in the output layer, and k denotes the quantity of hidden layers. The bias

term is defined by b_{ij} . z_{ij} represents the weight connection between the i -th input and the j -th output element given the input x . $M_i(x)$ is the most important feature value that can be extracted from the i -th element of the input vector in the process of mapping x to the output vector $M_i(x)$.

We employ the max pooling layer to decrease the parameter count within the fully connected layer. It conducts downsampling to diminish the dimensions of the feature map, effectively removing redundant data and decreasing the feature dimension. These characters help to speed up the computation speed. Additionally, for each distinct section of the input feature grid, the maximum value within that particular segment is selected as the output. Assume that the input feature map size is $h \times w$, the pooling window is $k_h \times k_w$, and the step size is $s_h \times s_w$, then the output feature map size is $\lfloor \frac{h-k_h}{s_h} \rfloor + 1 \times \lfloor \frac{w-k_w}{s_w} \rfloor + 1$. We consider the input feature as X , and designate the resulting feature map as Y , then

$$Y_{i,j} = \max_{X_{x,y}, (x,y) \in L_{i,j}} \quad (7)$$

where $L_{i,j}$ denotes the pooling window with (i, j) as the upper left corner.

The Flatten layer transforms multidimensional data into a singular one-dimensional structure before passing it to the fully connected layer. Moreover, recognizing the limited capacity of a single fully-connected layer in addressing nonlinear problems, we utilize two fully-connected layers to improve the overall efficacy of the model.

Then, we add a Dropout module to prevent overfitting. It operates by randomly activating hidden nodes and excluding them during each training batch, fostering diverse training networks that are not exclusively dependent on particular features. Employing such a strategy enhances the model's ability to generalize. Besides, the setting of the Dropout value also affects the experimental results. This paper uses a Dropout value of 0.5 in convolutional and fully connected layers.

Dropout is applied in both convolutional and fully connected layers. Unlike dropping out individual element values in the fully connected layer, the convolutional layer employs dropout by discarding the entire feature map. Therefore, our model introduces residual blocks to capture information from the feature maps that are dropped out by the convolutional layer. Residual blocks can alleviate the problem of vanishing gradients. Furthermore, by adjusting the proportion of the convolutional layer, the residual block can learn more feature values, thereby improving classification accuracy. In our model, the outputs of the first and second convolutions are summed as the input to the third convolution. Likewise, the fourth and fifth convolutional layers generate combined outputs and serve as the input to the subsequent sixth convolutional layer.

The Softmax activation is positioned after the second fully connected layer in the model. This mechanism can transform the predicted outcomes using an exponential operation to ensure positive outputs. Then, it normalizes the results to present them as probabilities, where the sum of all classification probabilities equals 1. The expression of the Softmax function is as follows:

$$Softmax = \frac{e^{Z_i}}{\sum_{m=1}^M e^{Z_m}} \quad (8)$$

TABLE I
TS-DRN PARAMETER

Layer	Hyper-parameters	Output shape
Input	-	29×30
Convolution	k:(3,3), s:(1,1), p:(1,1)	29×30@32
Convolution	k:(3,3), s:(1,1), p:(1,1)	29×30@32
Concat	-	29×30@32
Convolution	k:(3,3), s:(1,1), p:(1,1)	29×30@64
Max pooling	k:(2,2), s:(2,2), p:(1,1)	15×15@64
Convolution	k:(3,3), s:(1,1), p:(1,1)	13×13@64
Convolution	k:(3,3), s:(1,1), p:(1,1)	13×13@64
Concat	-	13×13@64
Convolution	k:(3,3), s:(1,1), p:(1,1)	13×13@128
Max pooling	k:(2,2), s:(2,2), p:(1,1)	7×7@128
Flatten	-	6272
Fully-connected	-	512

where Z_i represents the i -th prediction outcome, and m is the total number of predictions.

To optimize the training process of the model, we add the Adam function in the last part of the model as the optimizer. The Adam function dynamically adapts the learning rate for each parameter throughout the model's training, enhancing both convergence speed and the model's generalization capability. Simultaneously, the Adam function takes into account the estimation of both the first-order and second-order moments of the gradient. It makes the parameter update of the model smoother and avoids oscillation and instability. The calculation formula of the Adam function is as follows:

$$m_t = \beta_1 m_{t-1} + (1 - \beta_1) g_t \quad (9)$$

$$v_t = \beta_2 v_{t-1} + (1 + \beta_2) g_t^2 \quad (10)$$

$$\hat{m}_t = \frac{m_t}{1 - \beta_1^t} \quad (11)$$

$$\hat{v}_t = \frac{v_t}{1 - \beta_2^t} \quad (12)$$

$$\theta_t = \theta_{t-1} - \alpha \frac{\hat{m}_t}{\sqrt{\hat{v}_t} + \varepsilon} \quad (13)$$

where m_t and v_t denote the gradient first-order and second-order moment estimates, \hat{m}_t and \hat{v}_t are the corrected first-order and second-order moments, and α is the learning rate. We set $\alpha = 10^{-5}$, θ_t is the updated parameter, β_1 and β_2 are hyperparameters, and ε serves as a minute constant implemented to safeguard the denominator from becoming 0. Table I displays the detailed specifications of the model's parameters.

C. Cross-validation

Cross-validation is a widely employed technique for assessing a model's generalization performance. It can fully use the samples in the dataset to improve the model performance. The fundamental concept involves dividing the dataset into numerous subsets. While one subset serves as the test set, the rest of the subsets serve as the training set. The iterative training iteration is conducted multiple times, and the average is taken as the evaluation metric for the model. K-fold cross-validation stands out as the prevalent approach in cross-validation methodologies. K-fold cross-validation partitions the dataset into K different subsets in a randomized manner. In each iteration, one subset is designated as the test set, while the remaining K-1 subsets serve as the training set.

We iterate through this procedure K times (Each subset is used as a test set once and only once.) and compute the average of the validation results over K iterations as the model's performance metric.

IV. RESULTS

A. Evaluation indicator

This article employs metrics such as accuracy, precision, recall, and F1-score for evaluating performance. Their formulas are as follows:

$$accuracy = \frac{TP + TN}{TP + FP + TN + FN} \quad (14)$$

$$precision = \frac{TP}{TP + FP} \quad (15)$$

$$recall = \frac{TP}{TP + FN} \quad (16)$$

$$F1 - score = \frac{2 \times precision \times recall}{precision + recall} \quad (17)$$

where TP represents the count of true positives, TN represents the count of true negatives, FP represents the count of false positives, and FN represents the count of false negatives.

B. Experimental setup

This study implements the model on Windows 10 OS, IntelCore i7-12700, 2.3GHz CPU, 16GB RAM, and NVIDIA GeForce RTX 3050 Ti Laptop GPU platform. The programming language is Python, and the deep learning framework is Tensorflow.

C. Time-Slicing strategy

We perform segmentation due to the elevated dimensionality in the complete EEG signal features during the decision-making process of subjects. This process aims to mitigate feature dimensionality while concurrently augmenting the sample size. Fig. 6 represents the two-dimensional feature maps formed by slicing the EEG signals during a single decision-making instance of subject 07. Each input sample (3480) corresponds to each subject's EEG signal data collected during a single decision-making instance. After the slicing operation, this results in the generation of four feature maps, each with dimensions of 29×30 .

D. Comparing different Time-Slicing method

Different from the previous slicing method, we make the slicing step size (s) less than or equal to the sliding window (w). To find the optimal timing slice, we set the window size as a constant ($w = 870$) [43], with the step size denoted as a variable (s). $s \leq w$ not only allows us to obtain more slice samples, we can also learn the relevant features of their overlapping parts. We experiment with the step sizes of 100, 200, 300, 400, 500, 600, 700, 800, and 870 for slicing. We input the resulting slices into our classifier and then analyze the classification outcomes to determine the most effective sequential slicing approach. When $s=w=870$, it is the maximum value of the step size. At this time, the slices are independent of each other and ensure that the

model extracts all features in the EEG signal. Slicing at this step size can also be used as a comparison between previous slicing method and the Time-Slicing strategy of this article. We employ a 16-fold cross-validation approach, where each subject's sequential sample set serves as the test set in rotation, while the sequential slice sample sets of the remaining 15 subjects act as the corresponding training sets. The detailed classification accuracies are presented in Table II. Based on the information presented in Table II, we observe that when the sequential s is set to 500, 600, 700, and 800, the classification accuracy is higher than that with a step size of 870. These results indicate that the Time-Slicing strategy ($s < w$) outperforms the previous method ($w = s$). Among these step sizes, a step size of 700 achieves the highest classification accuracy, reaching 85.8%. Furthermore, when the step sizes are set to 100, 200, 300, and 400, the classification accuracy is lower than that with a step size of 870. We speculate this is due to a significant disparity between the step and window sizes, leading to a high overlap between slices. Our model magnifies misclassification probabilities and correct classification simultaneously during the classification process, decreasing classification accuracy overall.

Next, we select representative data (We compare the slice classification results for Subject 05, Subject 11, Subject 14, and Subject 15.) and create Fig. 7. It displays the classification accuracy of the four subjects under different step sizes, along with the corresponding training and test loss values. The bar chart shows that the classification accuracy follows a distribution closely resembling a normal distribution, with the highest accuracy achieved at a step size of 700, representing the optimal time-slicing proposed in this study. The line chart shows that the test set loss value is slightly higher than the training set loss value. However, the gap between them is relatively small, indicating that our model has strong generalization ability and good fit.

E. Comparison with common classifiers

In our study, we compare various standard classification models, including Support Vector Machine (SVM), Random Forest (RF), Adaptive Boosting (AdaBoost), Recurrent Neural Network (RNN), and our proposed Time-Slicing and Deep Residual Network (TS-DRN) model. We utilize the optimal time-series slices of EEG features acquired in the preceding sections as inputs for individual classifiers. The specific classification results are presented in Table III. Table III shows that RNN and our TS-DRN model exhibit excellent classification accuracy, significantly outperforming the other three traditional machine learning classifiers. This finding indicates that deep learning performs better on our dataset compared to conventional machine learning methods, demonstrating superior classification performance. Our model shows lower classification accuracy compared to RNN for subject 15, whereas, our model demonstrates superior overall performance in the realm of classification. To better represent these results, we select four representative subjects (Subject 04, Subject 07, Subject 11 and Subject 13.), extract their classification results, and visualize them in Fig. 8 to more intuitively present each model's performance.

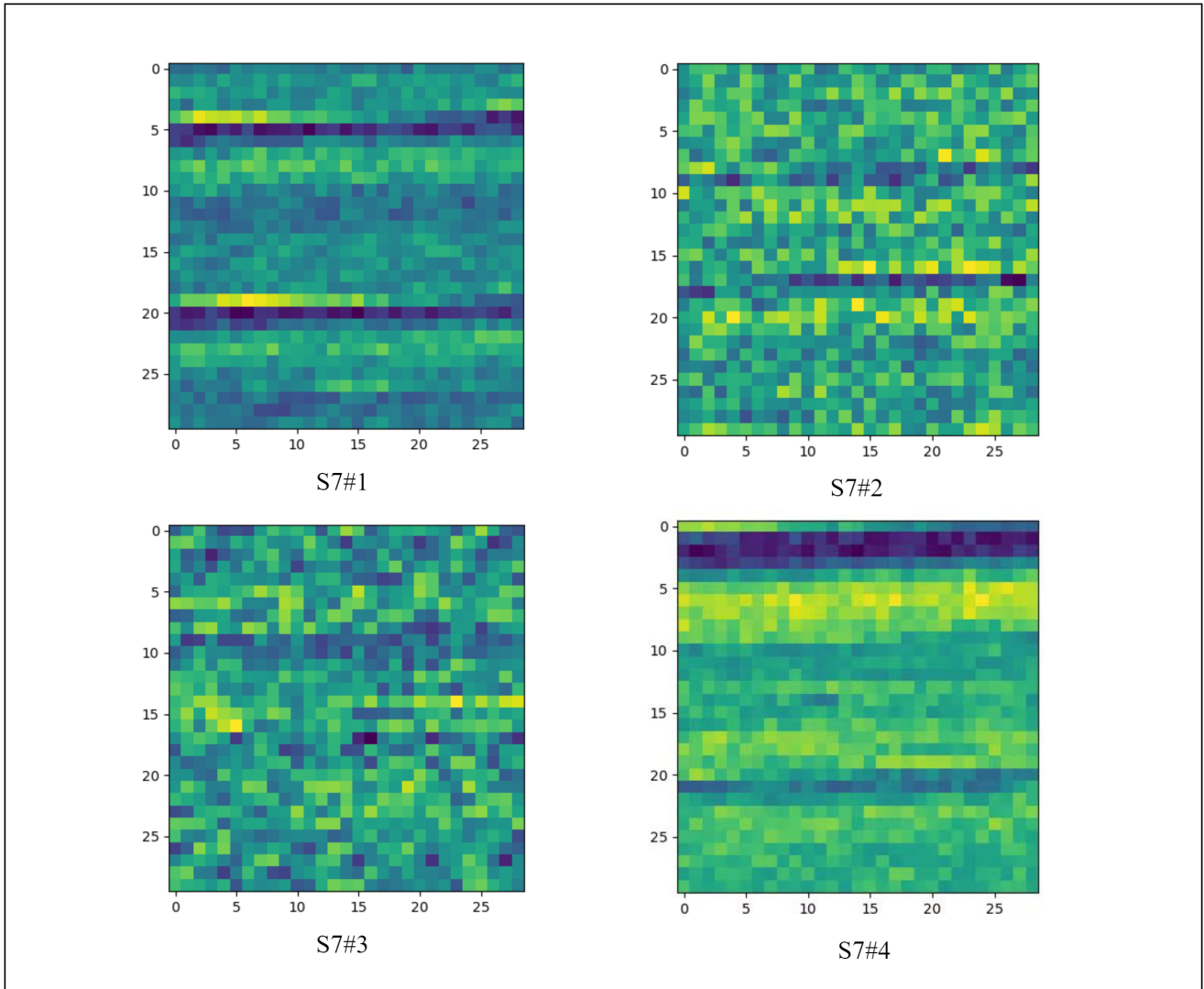


Fig. 6. Visualization of temporal slices of EEG signals during a single design decision in subject 7

TABLE II
COMPARISON OF CLASSIFICATION ACCURACY AT DIFFERENT TIME SERIES SLICES

Subject	100	200	300	400	500	600	700	800	870
S01	0.536	0.765	0.642	0.778	0.721	0.782	0.854	0.792	0.771
S02	0.742	0.654	0.721	0.772	0.778	0.791	0.831	0.781	0.763
S03	0.562	0.533	0.579	0.645	0.741	0.736	0.874	0.724	0.736
S04	0.681	0.742	0.755	0.818	0.759	0.837	0.865	0.773	0.685
S05	0.678	0.697	0.664	0.715	0.723	0.731	0.902	0.741	0.739
S06	0.665	0.546	0.603	0.736	0.729	0.796	0.838	0.790	0.785
S07	0.542	0.681	0.723	0.787	0.775	0.822	0.845	0.795	0.772
S08	0.746	0.749	0.763	0.723	0.745	0.769	0.824	0.764	0.776
S09	0.597	0.643	0.678	0.732	0.765	0.786	0.818	0.792	0.784
S10	0.632	0.675	0.669	0.628	0.673	0.718	0.845	0.701	0.681
S11	0.678	0.717	0.794	0.754	0.737	0.797	0.876	0.772	0.748
S12	0.658	0.664	0.632	0.654	0.689	0.794	0.839	0.763	0.682
S13	0.579	0.631	0.763	0.771	0.778	0.789	0.853	0.798	0.742
S14	0.632	0.648	0.658	0.675	0.703	0.712	0.894	0.715	0.721
S15	0.665	0.668	0.678	0.642	0.689	0.732	0.886	0.742	0.737
S16	0.665	0.668	0.678	0.642	0.689	0.732	0.886	0.742	0.737
Average	0.646	0.672	0.692	0.723	0.735	0.769	0.858	0.764	0.725

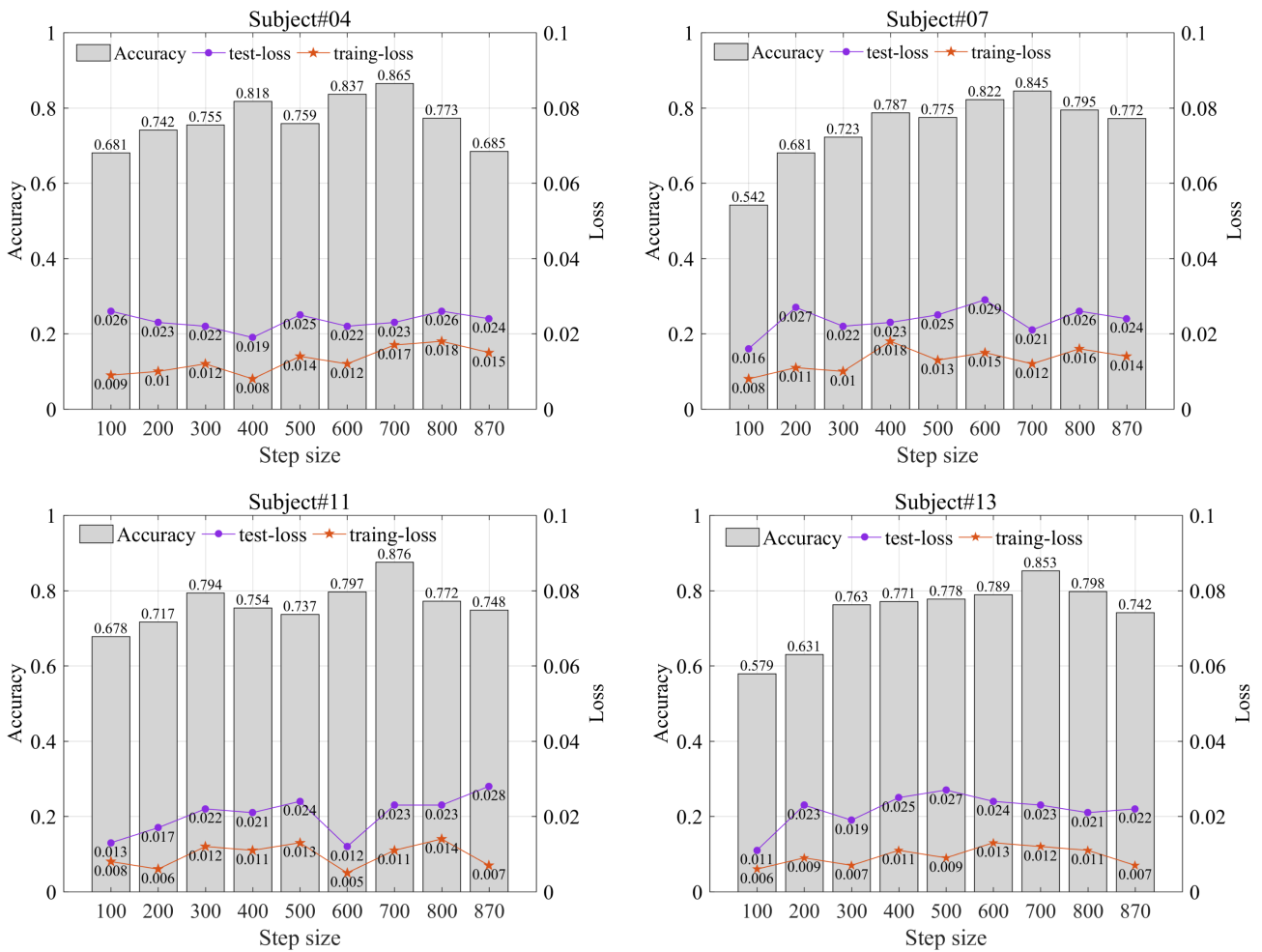


Fig. 7. Time-series slices of subject 04, subject 07, subject 11, and subject 13

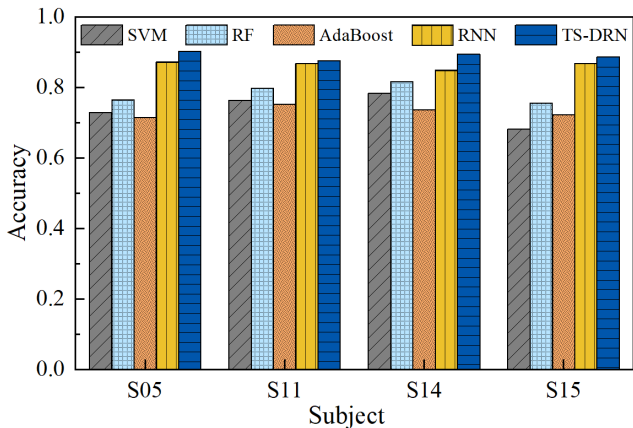


Fig. 8. Comparison of EEG data of some subjects in TS-DRN with SVM, Random Forest, AdaBoost and RNN models

F. Ablation experiment

We employ ablation experiments to investigate the function of residual blocks within the model. The TS-DRN model contains two residual blocks, and we investigate their effects on classification accuracy separately. Therefore, we design three variants of the TS-DRN model, V1,V2,V3. V1 is a model variant which removed the first residual block of the TS-DRN model. V2 is another model variant which removed

the second residual block of the TS-DRN model. V3 is the model variant which removed the two residual blocks of the TS-DRN model. We explore their contribution to the model by comparing their classification accuracies of EEG signals. The classification outcomes of the TS-DRN model and its three variants are depicted in Table IV and visualized in Fig. 9. Fig. 9 illustrates that the TS-DRN model attains the highest level of classification accuracy. The model with one residual block (V1 and V2) removed is inferior to our model. The model without residual blocks (V3) has the lowest classification accuracy. Hence, we draw the conclusion that integrating residual blocks enhances the model’s performance, with the optimal EEG signal classification achieved when two residual blocks are incorporated.

G. Comparison of Subjects with Different Educational Background

We recruit nine undergraduate students and seven graduate students as our subjects. Since groups of students at different learning stages have different educational experiences and knowledge reserves, we speculate that their EEG signal are different when making decisions. Therefore, we divide all subjects into undergraduate group and graduate group. Subsequently, we investigate the distinctions in EEG signals between the two groups during decision-making by assessing and contrasting their classification accuracy. We

TABLE IV
COMPARISON OF THE CLASSIFICATION ACCURACY OF TS-DRN AND THE THREE VARIANTS

subject	V1	V2	V3	TS-DRN
S01	0.756	0.765	0.723	0.854
S02	0.775	0.768	0.722	0.831
S03	0.783	0.778	0.715	0.874
S04	0.796	0.749	0.707	0.865
S05	0.727	0.801	0.743	0.902
S06	0.755	0.772	0.731	0.838
S07	0.768	0.745	0.725	0.845
S08	0.758	0.736	0.716	0.844
S09	0.779	0.784	0.713	0.838
S10	0.764	0.764	0.717	0.845
S11	0.757	0.755	0.720	0.876
S12	0.766	0.771	0.706	0.839
S13	0.772	0.769	0.721	0.853
S14	0.795	0.781	0.738	0.894
S15	0.762	0.769	0.734	0.886
S16	0.743	0.737	0.719	0.837
average	0.766	0.765	0.721	0.858

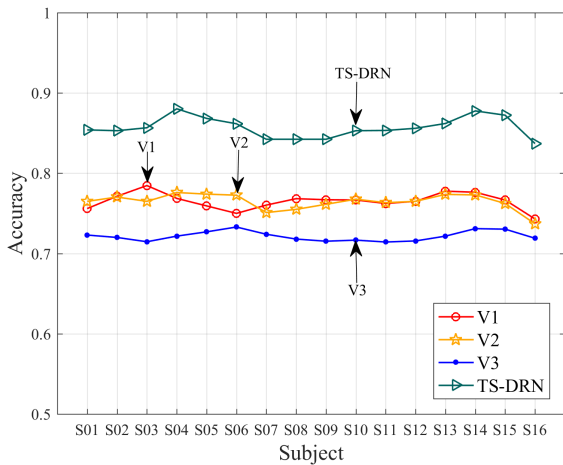


Fig. 9. Comparison of classification accuracy of TS-DRN and three variants

split the data from both groups into training and testing datasets, following an 8:2 distribution. Detailed outcomes of the specific classifications can be found in Table V. The classification accuracy for undergraduate students is 87.1%, higher than that of graduate students' classification accuracy. This difference in classification accuracy may be attributed to graduate students receiving more specialized academic training. Therefore, they exhibit greater cognitive flexibility regarding brain functionality and may engage in more comprehensive problem-solving approaches. These elements potentially lead to more complex brainwave signals, making the classification task for brainwave recognition algorithms more challenging.

Next, We plot the classification of EEG data for graduate students and undergraduate students into confusion matrices, as shown in Fig. 10. We compute precision, recall, and F1-score for both groups by analyzing the confusion matrices. The results for undergraduate students are presented in Table VI, while the corresponding results for graduate students are presented in Table VII. Comparing Table VI and Table VII, it becomes evident that the undergraduate cohort demonstrates higher precision, recall, and F1-score values. These results further illustrate that the EEG signals of the graduate student group are more difficult to identify than the EEG signals of the undergraduate group.

V. DISCUSSION

In Table VIII, as shown, we compare our approach with methods from existing literature. The study [27] used a densely connected convolutional neural network to classify EEG signals, achieving a maximum classification accuracy of 75.16%. In the study[44], EEG signals recorded during game decision-making were collected, and SVM was applied to classify them based on selected features, achieving a maximum accuracy of 80%. In the study[45], a model based on CNN combined with Dempster-Shafer (D-S) was proposed for EEG data classification, achieving a classification accuracy of 84%. In the study[26], a graph convolutional neural network was used to identify EEG signals from drivers during simulated driving, with a maximum binary classification accuracy of 91.5% and a three-class accuracy of 75.26%. However, our model performs a four-class

TABLE III
COMPARISON OF CLASSIFICATION ACCURACY OF SVM, RF, ADABOOST, RNN AND TS-DRN

Subject	SVM	RF	AdaBoost	RNN	TS-DRN
S01	0.702	0.765	0.609	0.828	0.854
S02	0.783	0.840	0.711	0.719	0.831
S03	0.788	0.789	0.648	0.831	0.874
S04	0.750	0.834	0.591	0.753	0.865
S05	0.729	0.765	0.714	0.871	0.902
S06	0.732	0.789	0.696	0.841	0.838
S07	0.711	0.753	0.720	0.832	0.845
S08	0.741	0.852	0.699	0.782	0.844
S09	0.732	0.822	0.729	0.808	0.838
S10	0.810	0.777	0.642	0.795	0.845
S11	0.763	0.798	0.752	0.867	0.876
S12	0.777	0.807	0.639	0.721	0.839
S13	0.802	0.822	0.744	0.793	0.853
S14	0.783	0.816	0.736	0.848	0.894
S15	0.682	0.755	0.723	0.867	0.886
S16	0.782	0.804	0.780	0.853	0.837
Average	0.754	0.799	0.696	0.813	0.858

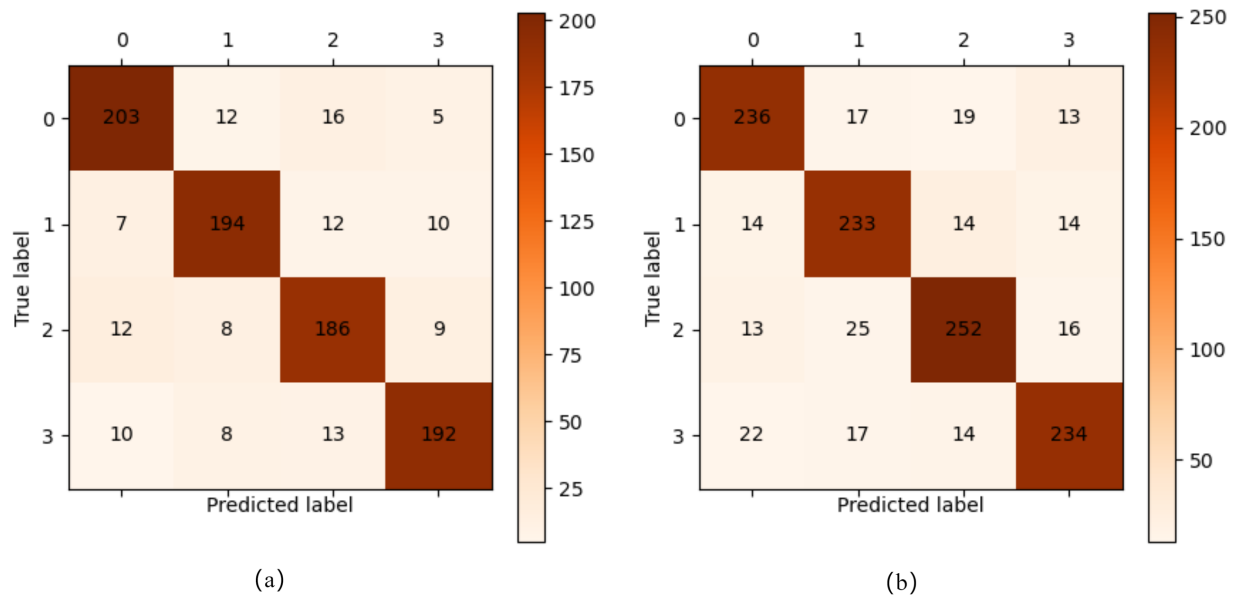


Fig. 10. Graduate and undergraduate students’ confusion matrix. Fig. (a) shows the confusion matrix for seven undergraduate students, Fig. (b) shows the confusion matrix for nine graduate students

TABLE V
COMPARISON OF CLASSIFICATION ACCURACY BETWEEN UNDERGRADUATE AND GRADUATE STUDENTS

educational background	accuracy
undergraduate	0.871
post graduate	0.832

TABLE VI
PRECISION, RECALL AND F1-SCORE FOR FOUR DECISIONS IN UNDERGRADUATE POPULATIONS

Evaluation metric	0	1	2	3
precision	0.875	0.874	0.857	0.889
recall	0.860	0.870	0.865	0.861
F1-score	0.868	0.872	0.861	0.875

classification on EEG signals, and outperforms the three-class model in classification performance. In the study[1], researchers collected subjects’ eye-tracking and EEG signals and then used a maximum strategy to classify fused features, achieving a maximum classification accuracy of 92.45%. However, if they only used EEG features for classification, the accuracy was 75.23%.

Based on the above analysis, considering the four classification results based on EEG signals, our approach demonstrates greater practicality and feasibility.

TABLE VII
PRECISION, RECALL AND F1-SCORE FOR FOUR DECISIONS IN GRADUATE POPULATIONS

Evaluation metric	0	1	2	3
precision	0.828	0.798	0.843	0.845
recall	0.828	0.847	0.824	0.815
F1-score	0.828	0.822	0.833	0.830

TABLE VIII
COMPARISON OF EEG SIGNAL CLASSIFICATION ALGORITHMS

Study	method	accuracy
Zhang et al.[27]	SVM	80%
Bo et al.[44]	PSD	92.45%
Zhang et al.[45]	CNN	75.16%
Chen et al.[26]	ETNN	84%
Wang et al.[1]	GNN	91.86%
ours	TS-DRN	85.8%

Furthermore, compared to other classification methods, although the TS-DRN model shows certain advantages in classifying EEG signals, it also has some limitations. These deficiencies may be because our approach solely relies on the temporal features of EEG signals for classification, resulting in a slightly lower classification performance than the multimodal fusion methods in the existing literature. Therefore, in the future, we will extract features from multiple domains as inputs to our model to enhance the model’s classification accuracy further.

VI. CONCLUSION

This paper introduces the TS-DRN (the Time-Slicing and Deep Residual Network) recognition model for classifying EEG datas related to art design decisions. We propose a Time-slicing strategy to extract EEG features which are fed into our deep residual network. We experiment with different time-slicing step sizes to find the optimal time-slicing for achieving the best classification results. Our model attains an average accuracy rate of 85.8% when classifying EEG signals, surpassing the performance of typical classification models. However, this study also has certain limitations. In the next steps of our research, we plan to address the following areas: (1) We will analyze both frequency-domain

and spatial-domain features from our dataset to obtain a more comprehensive set of EEG characteristics. (2) We will further optimize our network architecture, fine-tune relevant parameters, and explore integrating other deep learning methods, such as GCN, to enhance classification accuracy further.

REFERENCES

- [1] Y. Wang, S. Yu, N. Ma, J. Wang, Z. Hu, Z. Liu, and J. He, "Prediction of Product Design Decision Making: An Investigation of Eye Movements and EEG Features," *Advanced Engineering Informatics*, vol. 45, 2020.
- [2] M. Cao, C. Yang, and P. Y. Zhou, "Research on Bike Design Decision in the Post Sharing Era Based on KANO Model—From the Perspective of Designers and Consumers," *Packing Engineering*, vol. 43, pp. 395-404, 2022.
- [3] M. Antioco, R. Moenaert, and A. Lindgreen, "Reducing Ongoing Product Design Decision-making Bias," *Journal of Product Innovation Management*, vol. 25, no. 6, pp. 528-545, 2010.
- [4] J. Zhang, A. Simeone, P. Gu, and B. Hong, "Product Features Characterization and Customers Preferences Prediction Based on Purchasing Data," *CIRP Annals*, vol. 67, no. 1, pp. 149-152, 2018.
- [5] R. Ireland and A. Liu, "Application of Data Analytics for Product Design: Sentiment Analysis of Online Product Reviews," *CIRP Journal of Manufacturing Science and Technology*, vol. 23, pp. 128-144, 2018.
- [6] B. Peng, W. F. Wang, and J. Q. Hu, "Research on Decision Support System for Green Building Design-Based on the Integration of Ontology and Case Based Reasoning Technology," *Construction Economics*, vol. 09, pp. 81-88, 2023.
- [7] L. Zhu, Q. Yang, and T. Wu, "Emotion Analysis of Brain Waves Based on CNN and Bi-LSTM," *Journal of Applied Sciences*, vol. 40, no. 1, pp. 12, 2022.
- [8] G. Aurup and A. Akgunduz, "Preference Extraction from EEG: An Approach to Aesthetic Product Development," *Proceedings of the 2012 International Conference on Industrial Engineering and Operations Management*, Istanbul, Turkey, vol. 7, pp. 1178-1186, 2012.
- [9] Y. J. Si, X. Wu, F. Li, L. Zhang, K. Y. Duan, P. Y. Li, L. M. Song, Y. L. Jiang, T. Zhang, Y. S. Zhang, J. Chen, S. Gao, B. Biswal, D. Z. Yao, and P. Xu, "Different Decision-Making Responses Occupy Different Brain Networks for Information Processing: A Study Based on EEG and TMS," *Cerebral Cortex*, vol. 29, no. 10, pp. 4119-4129, 2019.
- [10] J. Shen, N. Liu, D. Li, and B. Zhang, "Behavioral Analysis of EEG Signals in Loss-Gain Decision-Making Experiments," *Behavioural Neurology*, vol. 2022, pp. 11, 2022.
- [11] Z. Liang, X. Zhang, R. Zhou, L. Zhang, L. Li, G. Huang, and Z. Zhang, "Cross-individual Affective Detection Using EEG Signals with Audio-visual Embedding," *Neurocomputing*, vol. 510, pp. 107-121, 2022.
- [12] L. Zong and N. Wang, "A Product Modeling Design Decision Model Based on PGA Genetic Algorithm," *Mathematical Problems in Engineering*, vol. 2022, 2022.
- [13] S. Zhu, J. Qi, J. Hu, and S. Hao, "A New Approach for Product Evaluation Based on Integration of EEG and Eye-tracking," *Advanced Engineering Informatics*, vol. 52, 2022.
- [14] Chew, L. H., J. Teo, and J. Mountstephens, "Aesthetic Preference Recognition of 3D Shapes Using EEG," *CognNeurodyn*, vol. 10, no. 2, pp. 165-173, 2016.
- [15] S. Lou, Y. Feng, G. Tian, Z. LvZ. Li, and J. Tan, "A Cyber-Physical System for Product Conceptual Design Based on an Intelligent Psycho-Physiological Approach," *IEEE Access*, vol. 5, no. 99, pp. 5378-5387, 2017.
- [16] S. Lou, Y. Feng, Z. Li, H. Zheng, and J. Tan, "An Integrated Decision-making Method for Product Design Scheme Evaluation Based on Cloud Model and EEG Data," *Advanced Engineering Informatics*, vol. 43, 2020.
- [17] P. Golnar-Nik, S. Farashi, and M. Safari, "The Application of EEG Power for the Prediction and Interpretation of Consumer Decision-making: A Neuromarketing Study," *Physiology & Behavior*, vol. 207, pp. 90-98, 2019.
- [18] S. Kumar, M. Yadava, and P. Roy, "Fusion of EEG Response and Sentiment Analysis of Products Review to Predict customer Satisfaction," *Information Fusion*, vol. 52, pp. 41-52, 2019.
- [19] S. Chang, W. Dong, and H. Jun, "Use of Electroencephalogram and Long Short-term Memory Networks to Recognize Design Preferences of Users Toward Architectural Design Alternatives," *Journal of Computational Design and Engineering*, vol. 7, no. 5, pp. 551-562, 2020.
- [20] H. J. Jiao, "Decision-making of Automobile Front Face Styling Features based on EEG Signals," *Mechanical Design*, vol. 02, pp. 134-139, 2023.
- [21] A. Bhardwaj, A. Gupta, and P. Jain, "Classification of Human Emotions from EEG Signals Using SVM and LDA Classifiers," *International Conference on Signal Processing and Integrated Networks*, vol. 2, pp. 180-185, 2015.
- [22] Z. Aishi, L. Zhang, X. Y. Yuan, and C. S. Li, "A Signal Prediction-based Method for Motor Imagery EEG Classification," *Biomedical Signal Processing and Control*, vol. 86, 2023.
- [23] B. KRisnAnDhikA, A. FAQih, and P. PuMAMAsARi, "Emotion Recognition System Based on EEG Signals Using Relative Wavelet Energy Features and A Modified Radial Basis Function Neural Networks," *Proceedings of 2017 International Conference on Consumer Electronics and Devices (ICCED)*, vol. 1, pp. 50-54, 2017.
- [24] Y. H. Geng and J. X. Shi, "Classification of Vertigo States by Combining Machine Learning and EEG Signal Analysis," *Tissue Engineering Research in China*, vol. 26, no. 29, pp. 4624-4631, 2022.
- [25] P. Dipti and S. Dhage, "Feature Extraction Methods for Electroencephalography based Brain-Computer Interface: A Review," *IAENG International journal of computer science*, vol. 47, no. 3, pp. 501-515, 2020.
- [26] J. L. Chen, X. F. Lin, W. F. Ma, Y. C. Wang, and W. i Tang, "EEG-based Emotion Recognition for Road Accidents in A Simulated Driving environment," *Biomedical Signal Processing and Control*, vol. 87, 2024.
- [27] J. Y. Zhang and K. Li, "A multi-view CNN Encoding for Motor Imagery EEG Signals," *Biomedical Signal Processing and Control*, vol. 85, 2023.
- [28] S. Tripathi, S. Acharya, R. Sharma, S. Mittal, and S. Bhattacharya, "Using Deep and Convolutional Neural Networks for Accurate Emotion Classification on DEAP Dataset," *In: Proc. of the 31st AAAI Conf. on Artificial Intelligence*, vol. 31, no. 2, pp. 4746-4752, 2017.
- [29] T. Song, W. Zheng, P. Song, and Z. Cui, "EEG Emotion Recognition Using Dynamical Graph Convolutional Neural Networks," *IEEE Trans. on Affective Computing*, vol. 11, no. 3, pp. 532-541, 2020.
- [30] K. M. He, X. Y. Zhang, S. Q. Ren, and J. Sun, "Deep Residual Learning for Image Recognition," *CoRR*, pp. 770-778, 2016.
- [31] C. J. Zheng, G. B. Xiao, and T. J. Luo, "Overlapping Time Slices to Improve Motion Imagery EEG Pattern Recognition by Deep Neural Networks," *Computer Systems Applications*, vol. 31, 2022.
- [32] J. Hwang, S. Park, and C. Jeonghee, "Improving Multi-Class Motor Imagery EEG Classification Using Overlapping Sliding Window and Deep Learning Model," *Electronics*, vol. 12, no. 1186, 2023.
- [33] G. Amir, A. Arbune, S. Beniczky, and P. Mierlo, "Evaluation of Ictal EEG Source Imaging with Sliding Window Approach to Localize the Epileptogenic Focus," *Clinical Neurophysiology*, vol. 141, 2022.
- [34] C. Zrenner, J. Tünnerhoff, C. Zipser, F. Müller-Dahlhaus, and U. Ziemann, "Brain-state Dependent Brain Stimulation: Real-time EEG Alpha Band Analysis Using Sliding Window FFT Phase Progression Extrapolation to Trigger An Alpha Phase Locked TMS Pulse with L millisecond Accuracy," *Brain Stimulation*, vol. 8, no. 2, pp. 378-379, 2015.
- [35] W. L. Zheng and B. L. Lu, "Investigating Critical Frequency Bands and Channels for EEG Based Emotion Recognition with Deep Neural Networks," *IEEE Trans. on Autonomous Mental Development*, vol. 7, no. 3, pp. 162-175, 2015.
- [36] S. Suhasini, M. Sridhar, S. Bandi, N. Chaitanya, M. Ahmed, and D. Nabamita, "EEG Signal Processing by Feature Extraction and Classification Based on Biomedical Deep Learning Architecture with Wireless Communication," *Optik*, vol. 270, 2022.
- [37] Y. Li, W. Zheng, Z. Cui, T. Zhang, and Y. Zong, "A Novel Neural Network Model Based on Cerebral Hemispheric Asymmetry for EEG Emotion Recognition," *In: Proc. of the 27th Int'l Joint Conf. on Artificial Intelligence*, vol. 27, pp. 1561-1567, 2018.
- [38] T. F. Song, W. M. Zheng, P. Song, and Z. Cui, "EEG Emotion Recognition Using Dynamical Graph Convolutional Neural Networks," *IEEE Trans. on Affective Computing*, vol. 11, no. 3, pp. 532-541, 2020.
- [39] S. E. Moon, S. Jang, and J. S. Lee, "Convolutional Neural Network Approach for EEG-based Emotion Recognition Using Brain Connectivity and its Spatial Information," *In: Proc. of the 2018 IEEE Int'l Conf. on Acoustics, Speech and Signal Processing (ICASSP)*. Calgary: IEEE, vol. 38, pp. 2556-2560, 2018.
- [40] H. Y. Xu and K. Plataniotis, "Affective States Classification Using EEG and Semi-supervised Deep Learning Approaches," *In: Proc. of the 18th IEEE Int'l Workshop on Multimedia Signal Processing (MMSP)*. Montreal: IEEE, vol. 20, pp. 1-6, 2016.
- [41] S. Tripathi, S. Acharya, R. Sharma, S. Mittal, and S. Bhattacharya, "Using Deep and Convolutional Neural Networks for Accurate Emotion Classification on DEAP Dataset," *In: Proc. of the 31st AAAI Conf. on Artificial Intelligence*. San Francisco: ACM, vol. 31, no. 2, pp. 4746-4752, 2017.

- [42] T. Zhang, W. M. Zheng, Z. Cui, Y. Zong, and Y. Li, "Spatial-temporal Recurrent Neural Network for Emotion Recognition," *IEEETrans*, vol. 49, no. 3, pp. 839-847, 2018.
- [43] H. Candra, M. Yuwono, R. Chai, A. Handojoseno, I. Elamvazuthi, H. Nguyen, and S. Su, "Investigation of Window size in Classification of EEG-emotion signal with Wavelet Entropy and Support Vector Machine," *2015 37th Annual international conference of the IEEE Engineering in Medicine and Biology Society (EMBC). IEEE*, vol. 12, pp. 7250-7253, 2015.
- [44] H. J. Bo, X. L. Liu, and L. Ma, "Time-frequency Characterization of EEG During Guessing Game and Prediction of Game Decision Based on Preferred Features," *Signal Processing*, vol. 33, pp. 273-279, 2017.
- [45] L. Zhang, F. Y. Xiao, and Z. H. Cao, "Multi-channel EEG Signals Classification Via CNN and Multi-head Self-attention on Evidence theory," *Information Sciences*, vol. 642, 2023.